Check for updates

View Article Online
View Journal

MSDE

Molecular Systems Design & Engineering

Accepted Manuscript

This article can be cited before page numbers have been issued, to do this please use: V. Y. Rudyak, A. A. Gavrilov, D. Guseva, S. Tung and P. V. Komarov, *Mol. Syst. Des. Eng.*, 2020, DOI: 10.1039/D0ME00034E.

This is an Accepted Manuscript, which has been through the Royal Society of Chemistry peer review process and has been accepted for publication.

Accepted Manuscripts are published online shortly after acceptance, before technical editing, formatting and proof reading. Using this free service, authors can make their results available to the community, in citable form, before we publish the edited article. We will replace this Accepted Manuscript with the edited and formatted Advance Article as soon as it is available.

You can find more information about Accepted Manuscripts in the Information for Authors.

Please note that technical editing may introduce minor changes to the text and/or graphics, which may alter content. The journal's standard Terms & Conditions and the Ethical guidelines still apply. In no event shall the Royal Society of Chemistry be held responsible for any errors or omissions in this Accepted Manuscript or any consequences arising from the use of any information it contains.

ROYAL SOCIETY OF CHEMISTRY
View Article Online
DOI: 10.1039/D0ME00034E

Molecular Systems Design & Engineering

PAPER

Published on 09 June 2020. Downloaded by Uppsala University on 6/13/2020 1:36:52 PM.

Design, System, Application

The growing demand for clean energy resources caused by increase in the Earth population and the related increase in the consumption of planet resources has made research, development, and production of both traditional and based on new materials solar cells relevant. One of the potential alternatives to crystalline silicon solar cells is organic photovoltaic cells made of thin films based on polymer materials, which can be easily applied layer by layer onto flexible substrates of large area using wet processing methods. The use of polymeric materials gives such promising advantages as ease of processing, possible recyclability, and relatively low cost. A typical structure of a polymer solar cell (PSC) has the multilayer architecture. For the widespread of polymer solar cells in daily practice, it is necessary to achieve a number of properties, such as the high power conversion efficiency, durability, and stability with prolonged exposure to temperature changes. When developing PSC, many polymeric materials need to be tested. The use of computer simulations can greatly facilitate the process of design and verification of the properties of various polymers prior to their experimental study. In studying the morphology of a photoactive layer (PL), which is crucial for PSC efficiency, the development of computer models is facing a significant challenge. The fact is that the PL is a nanocomposite in which π-conjugated (semiconducting) polymers are used as matrices. Due to π-π stacking interactions, crystalline domains, which play an important role in the formation of PL properties, are present in the structure of conjugated polymers. However, at present, computer simulation methods have very limited possibilities for constructing models of polymeric materials, taking into account π-π interactions driving self-assembly processes. This problem is especially acute for mesoscopic methods that allow the study of polymeric materials at relatively large length and time scales. In this paper, we propose a method for taking into account π-π stacking interactions in mesoscale models and check it in the framework of the dissipative particle dynamics method. We implement the dynamic bonding of mesoscopic particles in the model of conjugated polymer chains. As a prototype of polymer model, we use poly (3-hexylthiophene). We show that, taking into account π-π stacking interaction in our model leads to self-assembly of the polymer chains into large stacks with strong alignment due to the dynamic bonding. These stacks form lamellae, which is in good agreement with the known experimental data. The proposed methodology could be helpful in studies of conjugated polymer materials especially in design of PSC and other photovoltaic devices.

Molecular Systems Design & Engineering Accepted Manuscript

Please do not adjust margins

View Article Online
DOI: 10.1039/D0ME00034E

Journal Name

ARTICLE TYPE

Cite this: DOI: 00.0000/xxxxxxxxxx

Accounting for π–π Stacking Interactions in Mesoscopic Models of Conjugated Polymers

Vladimir Yu. Rudyak,*[a] Alexey A. Gavrilov,[a] Daria V. Guseva,[b] Shih-Huang Tung,[c] and Pavel V. Komarov[b,d]

Received Date
Accepted Date

DOI: 00.0000/xxxxxxxxxx

Conjugated polymer films play a decisive role in construction of photoactive elements in organic electronics devices. Their morphology is mainly determined by self-assembly processes during crystallization initiated by π-π interactions between aromatic rings. However, currently there are only very limited capabilities to construct polymer matrix models taking into account their crystallization in the framework of computer simulations. In this paper, we propose an extension of mesoscale modeling methodology based on dissipative particle dynamics method. We use poly(3-hexylthiophene) (P3HT) as a prototype of the mesoscopic model of polymer chains. To take into account the π-π interactions, we implement the formation and breaking of additional dynamic non-covalent bonds between coarse particles mapped to thiophene rings. We show that the introduction of dynamic bonds makes possible to simulate the self-assembly of the conjugated polymer chains into hexagonal packed cylinder morphology and lamellar morphology with large thiophene stacks.

1 Introduction

Bulk heterojunction plastic films based on polymer matrices belonging to p-type semiconductors (electron donors) and fillers consisting of n-type semiconductors (electron acceptors), such as n-type conjugated polymers, fullerenes, and quantum dots, are widely used to construct the organic photovoltaic devices, e.g., photodiodes, phototransistors, and solar cells (PSC) devices [1–4]. The latter attract increasing attention as promising renewable, environmentally friendly sources of cheap electric energy [5]. In addition to the chemical composition and molecular architecture of polymers, the morphology of the photoactive layer significantly affects the overall efficiency and thermodynamic stability of PSC [3,6].

Regioregular poly (3-hexylthiophene) (P3HT) (Fig. 1a), which belongs to the semiconducting polymers from the polythiophene family, is one of the most outstanding and the most studied electron-donor materials. Its popularity is primarily due to the relatively high mobility of charge carriers ($0.1\,cm^2/(V\times s)$) combined with a high degree of solubility [7,8]. P3HT has a rigid backbone chain with attached side alkyl chains that increase the solubility of the polymer in organic solvents [9]. The degree of P3HT crystallinity varies in the range of 60%–70% [7,9,10]. The equilibrium crystalline structure of poly (3-hexylthiophene) and its dependence on temperature and molecular weight is still disputed. The X-ray diffraction analysis (XRD) of P3HT films shows that the crystalline domains, consisting of stacked lamellae, alternate with amorphous polymer regions. The crystalline domains are formed via packing of thiophene rings into "stacks" due to the π-π stacking interactions. The following characteristic scales of the spatial organization of the crystalline domains were revealed: the scale of 3.8 Å correlates with the distance between the thiophene rings forming the stacks, the scale of 16 Å correlates with the distance between the P3HT chains separated by the side alkyl chains, the scale of 28 nm correlates with the spatial periodicity of the lamellar domains [7–10].

The presence of the crystalline domains in the conjugated polymers can strongly affect the morphology of the formed films, the mobility of charge carriers in them, and consequently the properties of produced electronic devices. Therefore, the theoretical consideration of such systems requires constructing computational models capable to reproduce the structure of crystallizing polymers with maximal possible accuracy. However, this is not easy to implement. The crystallization of polymers is kinetically controlled process that occurs under the thermodynamic conditions far from equilibrium state, so the crystal morphology (fibrils, lamellae, axialites or spherulites) depends on the interplay of surface tension and diffusion [11–13]. Even in the case of crystalliza-

[a] Faculty of Physics, Lomonosov Moscow State University, Leninskie Gory, 1-2, Moscow 119991, Russia.
[b] Nesmeyanov Institute of Organoelement Compounds, Russian Academy of Sciences, Vavilova st., 28, Moscow 119991, Russia.
[c] Institute of Polymer Science and Engineering, National Taiwan University, Taipei 10617, Taiwan.
[d] Tver State University, Sadovyj per., 35, Tver 170002, Russia.

† Electronic Supplementary Information (ESI) available: [details of any supplementary information available should be included here]. See DOI: 10.1039/cXsm00000x/

Published on 09 June 2020. Downloaded by Uppsala University on 6/13/2020 1:36:52 PM.

Molecular Systems Design & Engineering Accepted Manuscript

View Article Online
DOI: 10.1039/D0ME00034E

Published on 09 June 2020. Downloaded by Uppsala University on 6/13/2020 1:36:52 PM.

Molecular Systems Design & Engineering Accepted Manuscript

tion of linear flexible chain polymers, the sequence of transitions (occurring at different space and time scales) from strongly entangled states to highly ordered domains takes place. For these reasons, the crystallization process is a difficult problem to be described by rigorous analytical methods, especially for polymers with complex structure and the presence of specific intermolecular interactions such as hydrogen bonds and π-π stacking[13]. Today, due to the rapid growth in computer power, simulations have become an important method for the direct study of various processes in complex molecular systems. However, the use of full-atomic molecular mechanics methods such as molecular dynamics (MD) and Monte Carlo (MC) to describe the crystallization processes is limited by the size of the model samples and the duration of their simulations due to the very slow dynamics of these processes. Up to now, the crystallization of polymers and the preceding stages have been modeled in detail only for linear polymers in the framework of coarse-grained models[14–17]. Such modeling in the framework of full-atomic models is performed mainly for single chains[18]. For the polymer matrices the technique is applied only in the framework of the united-atoms models[19,20].

To describe the properties of conjugated polymers, it is necessary to take into account the π-π stacking interaction in computer models. It acts over short distances, has a strong spatial orientation, and it is strong enough to force molecules to self-assemble into highly ordered supramolecular structures called aggregates or stacks. Owing to these features, the polymer chains become effectively rigid, which reveals itself in the increased chain's persistent length. In the case of P3HT, its estimated value ranges from 21 Å to 33 Å[9,21,22]. Due to the short intermolecular distances in the stacks, new overlapping molecular orbital levels are created, which contribute to the delocalization of electrons and to the transfer of charge carriers[2]. Since π-π interactions are caused by specific electron correlations[23,24], the effect of such interactions is difficult to extrapolate to molecular mechanics methods. In the force fields of molecular mechanics, to some extent, π-π interactions are taken into account by adjusting the partial charges and van der Waals (vdW) interactions of atoms in the composition of aromatic rings[23–26]. But this approach cannot fully reproduce the directional effect of π-π interactions on the conjugated polymer morphology formation. In mesoscopic simulations, the problem of taking into account the π-π stacking interactions is poorly investigated[27–34]. One of the most successful ways is based on using soft anisotropic nonbonded interactions, which strikes certain difficulties in modeling large systems[35].

Up to now, the structure of P3HT has been repeatedly studied using the computer simulation in the framework of various approximations from the coarse-grained models to the full-atom ones[27–35]. In these studies, the crystallization process was considered as a consequence of the stiffness of the polymer chain and the specificity of the intermolecular interaction between coarse-grained particles or united atoms. In this case, the alignment of the thiophene rings due to the π-π stacking is realized only within the framework of the united atoms models[34,36].

In our recent work,[37] we used the mesoscale modeling technique based on the dissipative particle dynamics (DPD) method[38], and studied the possibility to control the morphology of the photoactive layer by choosing the chemical structure of the blocks of the conjugated AB copolymer. As a prototype of one of the blocks we used P3HT. DPD method is effective when predicting the three-dimensional morphology of various polymer materials, which is the result of the self-assembly process[37–40]. The DPD method allows to track the evolution of sufficiently large molecular systems in the direction to the ordered thermodynamic equilibrium state due to reducing the internal degrees of freedom and using soft potentials but it does not explicitly take into account the π-π stacking interactions.

In the present work, we modify the DPD model of conjugated polymer chains by introducing additional dynamic non-covalent bonds to take into account the formation of supramolecular morphologies in the P3HT matrix caused by π-π stacking interaction. It should be noted that another important task in the simulation of conjugated polymers is to correctly take into account the conformational properties of polymer chains in particular by carefully fitting the torsion potentials[41–43]. However, in this study, to focus at the effect of π-π stacking self-assembly, we did not include torsion potentials in our model.

2 Methods

2.1 Coarse-grained model of P3HT

We used dissipative particle dynamics simulations to model a conjugated polymer matrix. DPD is a mesoscale simulation technique suggested by Hoogerbrugge and Koelman[44,45], and developed by Espanol, Groot, and Warren for simulations of polymers and molecular systems[38,45,46]. In this method, the polymer molecules are represented in terms of the bead-and-spring model, with particles governed by Newton's equations and interacting through a conservative force (repulsion), a dissipative force (friction), and a random force (heat generator). Each DPD bead has the same weight m and size σ. For weight, length, energy, and time, the reduced units $m = 1$, $\sigma = 1$, $k_BT = 1$ and $\tau = \left(\frac{m\sigma^2}{k_BT}\right)^{1/2}$ are used (T is absolute temperature, k_B is the Boltzmann constant). A soft repulsive potential enhances the stability of the integration of the equations of motion, allows to increase the time step (in comparison with molecular or Brownian dynamics), and thus to access to large time and spatial scales in the simulation of complex polymer systems. Recently, this method was successfully used to describe the structure and properties of various polymer systems[31,39,47,48]. It is also adopted for simulating chemical reactions and dynamic bonding between particles[49–53]. We omit the details of this method because they are well described in the publications mentioned. In addition, a recent review and comparison of different molecular scale simulations on thermoset polymers can be found in Ref. [54]. Hereinafter, the dimensionless units were used, which is common in coarse-grained simulations.

As a prototype of the mesoscopic model of a polymer chain, we used the chemical structure of poly (3-hexylthiophene). In this study, coarse-grained model of P3HT monomer consisted of one bead A (thiophene fragment) and three beads B (alkyl side chain), as shown in Fig. 1a, b). The system density was $\rho = 3\sigma^{-3}$. The simulations box contained 1012 polymer chains of length $N = 20$

View Article Online
DOI: 10.1039/D0ME00034E

Published on 09 June 2020. Downloaded by Uppsala University on 6/13/2020 1:36:52 PM.

Molecular Systems Design & Engineering Accepted Manuscript

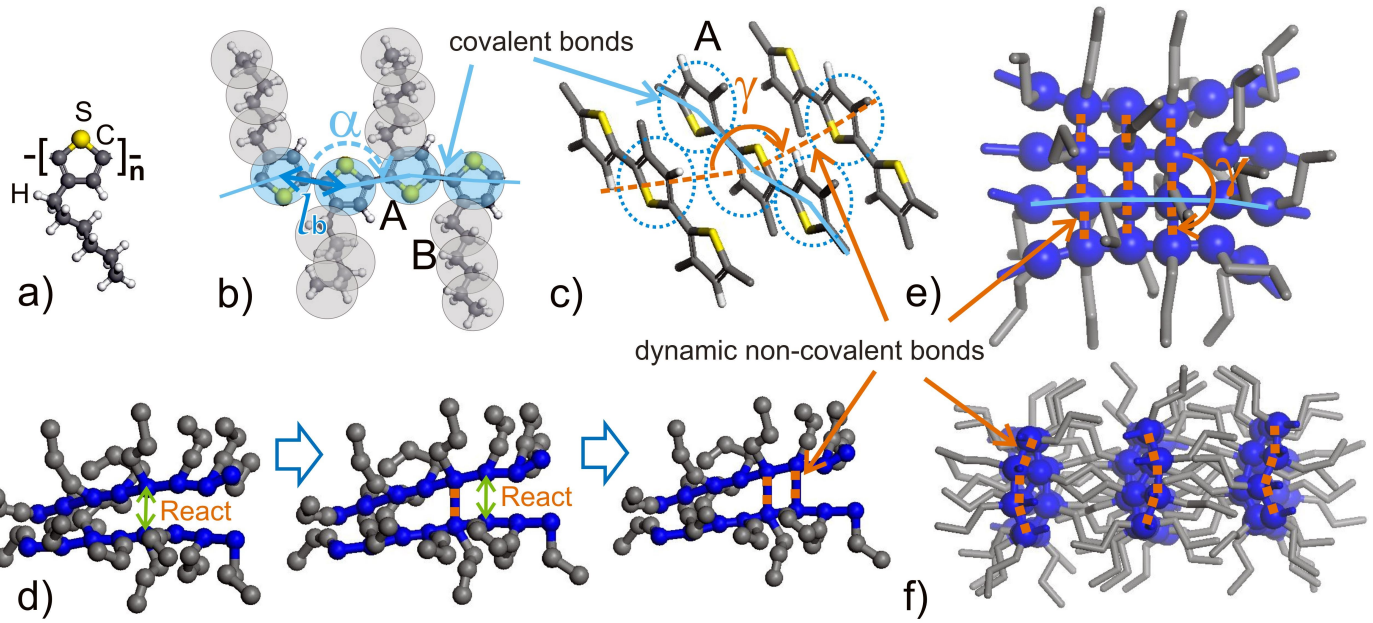

Fig. 1 a) Chemical structure of poly (3-hexylthiophene) monomer. b) The structure of a single P3HT chain in our coarse-grain model (blue solid lines depict covalent bonds between beads of the main chain). Schematic representation of c) a coarse-grained stack of thiophene rings belonging to different P3HT chains (orange dashed lines show dynamic non-covalent bonds, representing π-π stacking). d) the main stages of formation of the dynamic bonds. Visualization of P3HT stacks e) top view, f) side view. The valence angle, α, between the A-beads is introduced to control the persistence length of the main chain. l_b - equilibrium bond length. An additional valence angle $\gamma = 180°$, between the beads of adjacent chains is introduced to control the alignment of the chains in the stack relative to each other.

monomers and had size of $l_x \times l_y \times l_z = 30 \times 30 \times 30\sigma^3$ (here l_i is the simulation cell edge in i-th direction), which is approximately $17 \times 17 \times 17\,\mathrm{nm}^3$ (based on the mass of the equivalent atomistic system and the experimental density value for regioregular P3HT 1.15 g/cm^3 [9]). Thus, the DPD unit length σ is about 0.57 nm. The selected coarsening is a good compromise, since it allows to adequately reproduce the structural features of the polymer chain and to simulate the morphology of the system under conditions of solution and melt[31,33,55]. While we considered P3HT polymer in this study, we believe the model is widely applicable to other polythiophenes (for example, with different morphology of the sidechain and their arrangement) [56].

The DPD pair repulsion parameters a_{AA} and a_{BB} were equal to 100, while a_{AB} varied from 100 (no incompatibility between A and B) to 120 (high incompatibility between A and B). The test of the model at different degrees of compatibility between the backbone and side chains was done for better understanding of capability of the model to reproduce behaviour of polymers with various chemical structure. An evaluation of the repulsion parameter a_{AB} corresponding to the case of P3HT is described in Electronic Supplementary Information (ESI). The harmonic potential with equilibrium bond length $l_b = 0.5\sigma$ and bond strength $K_b = 50 k_B T/\sigma^2$ was applied to all bonds. Such combination of repulsion parameters and bond strength was used to avoid the formation of unnatural local structures. In addition, the harmonic valence angle potentials with equilibrium angle $\alpha_0 = 180°$ and of various stiffness K_A were applied to main chain to maintain its persistence length (which is governed by angle α, see Fig. 1(b)). The friction coefficient was $\gamma = 4.5\,\tau^{-1}$. For improved stability of the integration scheme we used for integration of equations of motion a time step $\Delta t = 0.01\,\tau$. No torsion potential was included in the interactions, thus we excluded from our model the effects of the regioregularity or the interdigitation of the side chains. At the same time, the model is fully compatible with torsion potentials, and the regioregularity of the polymer can be easily taken into account in the future.

2.2 π-π stacking via dynamic bonding

In our model, π-π interactions were introduced via dynamic bonding of main chain beads (of type A in Fig. 1). In this respect, our model resembles previous studies with saturating bonds[57]. The formation and breaking of dynamic non-covalent bonds between these beads were based on the concept of "mesoscale chemistry", in which reactions are probabilistic, see for details [52,58–60]. For this purpose at the beginning of simulations, beads of type A are assigned a valence number of 2 that means these beads can form two additional bonds between each other.

Two reactions were implemented: 1) dynamic bond formation reaction, and 2) dynamic bond breaking reaction. For dynamic bonds formation, we used the following algorithm. At regular intervals, for every bead i of type A with free valence (called primary bead below), the search for neighbor j satisfying the following conditions was performed (see Fig. 1d):

1. Bead j also has type A.
2. Bead j is within reaction radius $R_{\mathrm{react}} = 0.8\sigma$ from bead i.
3. Bead j has free valence.

View Article Online
DOI: 10.1039/D0ME00034E

Published on 09 June 2020. Downloaded by Uppsala University on 6/13/2020 1:36:52 PM.

4. Beads i and j are not already bonded.

5. If beads i and j belong to the same main chain, they are not closer than 3 bonds away from each other.

6. There is no another bead k in the system, which is bonded (statically or dynamically) to both beads i and j. In other words, the formation of triangles of bonds is forbidden.

Dynamic non-covalent bond formation and breaking procedures were executed consequently every 200 Δt DPD steps, which was enough to satisfy the local relaxation of the polymer chains[59,60]. When these procedures were triggered, the closest neighbor was chosen from the list of neighbors satisfying the conditions. With probability p_{create} the new dynamic bond was formed (equilibrium bond length $l_d = 0.5\,\sigma$, bond strength $K_d = 50\,k_bT/\sigma^2$, same as for regular bond). The new bond angles were added to take into account the high sensitivity of π-π bonds to the mutual position and orientation of the chains. These angles between the new dynamic bond and existing dynamic bonds are marked as γ in Fig. 1c and e, and are characterized by equilibrium angle $\gamma_0 = 180^\circ$ and angle strength $K_\gamma = 5\,k_bT/rad^2$. These angles, together with the steric interactions of neighbour particles, control the planar orientation of the stacks formed by multiple chains, see Fig. 1(f).

For dynamic non-covalent bond breaking, each existing dynamic bond were deleted with probability p_{break}, and the bond angles including this bond were also removed from the system. The bond breaking procedure was executed right after bond formation procedure, thus setting $p_{\text{break}} = 1$ led to the absence of dynamic bonds. The lower the value p_{break}, the more dynamic bonds were formed. The ratio $p_{\text{create}}/p_{\text{break}}$ has been varied from 1 to 10.

2.3 Simulations protocol and structural analysis

All simulations were performed using in-house DPD package previously used in many works, including[60–64]. Starting conformations were generated by randomly placing polymer chains in simulations box. Each system was equilibrated for $2\times10^8\Delta t$ steps ($2\times10^6\tau$ DPD time units). Then the structural properties were estimated during productive run of $0.5\times10^8\Delta t$ steps.

Static structure factor was calculated as

$$S(q) = \left\langle \frac{1}{n}\sum_{j=1}^{n}\exp\left(i\bar{q}\bar{r}_j\right)\right\rangle_{|\bar{q}|=q},$$

where n is the total number of particles, and averaging is performed over the wave vector set $q_x, q_y, q_z = 2\pi k/l_x, 2\pi m/l_y, 2\pi p/l_z$, where k, m, p are integers from 1 to 32, and over a sequence of independent system conformations. Conformations at frequency of 10^5 steps were taken for the averaging.

3 Results and discussion

The primary results of our simulations are the equilibrated phases of model melt of thiophene oligomers at various conditions. Even at the fixed architecture of model polymer, there are several model parameters that affect the resulting morphology of the system. Here, we focus on discussion of the effect of such parameters as the rigidity of main chains (which is governed by K_A), the miscibility between main and side chains (χ_{AB}), and the ratio of the formation and breaking of dynamic bonds ($p_{\text{create}}/p_{\text{break}}$). Supposedly, the exact values of these parameters can be extracted from quantum mechanical simulations for any certain thiophene polymer. At the same time, these values vary with temperature, sidechain structure, and additional compounds. Therefore, we were interested in exploring the regimes and morphologies, which the model allows to obtain, rather than in limiting the simulations to a single compound. For this purpose, we first studied the impact of each parameter independently. In the subsections below, we first report the behavior of the model without π-π interaction between thiophene particles. Second, we report the phase diagram of the system with π-π interaction (by allowing formation of various amounts of dynamic bonds) and chemical incompatibility between thiophene and side chains. Additionally, structural analysis of each obtained phase is shown. Finally, we present the mutual effect of dynamic bonding and main chain stiffness in the absence of chemical incompatibility between the system components to explore the limits of the model.

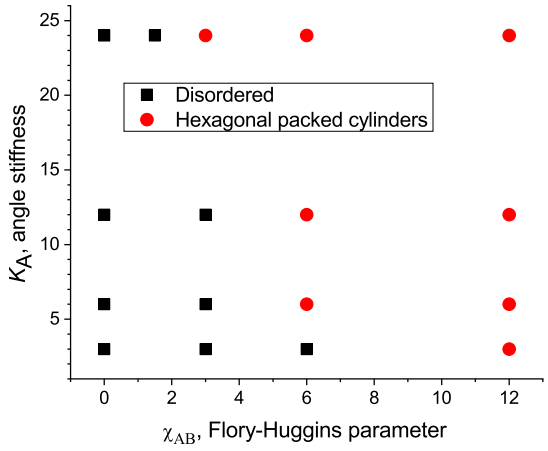

Fig. 2 Phase diagram of equilibrated systems at various angle stiffness K_A and incompatibility parameter for the main and side chains χ_{AB}. Dynamic non-covalent bonds are switched off (no π-π stacking). The value of $\chi_{\text{AB}} = 3$ corresponds to the case of P3HT (see ESI).

3.1 System behavior without dynamic bonding

First of all, we equilibrated the melt without dynamic non-covalent bonds. The chemical incompatibility between thiophene chains and side chains was simulated by the difference in DPD repulsion potential $\Delta a = a_{\text{AB}} - a_{\text{AA}}$. According to Ref. [38], we used the linear relation between Δa and Flory-Huggins parameter, viz., $\chi_{\text{AB}} \approx 0.3\Delta a$. We varied χ_{AB} from 0 to 12 (corresponding to Δa from 0 to 40). Angle stiffness of main chains K_A varied from $3\,k_bT/rad^2$ (soft chains) to $24\,k_bT/rad^2$ (rigid chains). The resulting phase diagram is shown in Fig. 2. At $\chi_{\text{AB}} = 0$, the system remained disordered after equilibration at all values of K_A (black squares in Fig. 2). Introduction of chemical incompatibil-

Molecular Systems Design & Engineering Accepted Manuscript

View Article Online
DOI: 10.1039/D0ME00034E

Published on 09 June 2020. Downloaded by Uppsala University on 6/13/2020 1:36:52 PM.

ity ($\chi_{AB} > 0$) leaded to the microphase separation and formation of hexagonal packed cylinders phase (red circles in Fig. 2) at high enough K_A or χ_{AB}. In contrast to the predictions of coarse-grained molecular dynamics model[30], soft DPD potential leads to the absence of lamellar morphology in reasonable range of parameters. Thus, the introduction of π-π stacking is required to obtain the morphological features of P3HT.

3.2 Effect of component incompatibility in system with dynamic bonding

To obtain morphologies with higher ordering we introduced dynamic bonding between neighbor thiophene chains. The balance between bond formation and breaking can be expressed by the dynamic bonding rate p_{create}/p_{break}, which effectively regulates the amount of dynamic bonds in the system. We varied p_{create}/p_{break} from 1 to 10. Dynamic bonding rate $p_{create}/p_{break} = 1$ leads to the absence of dynamic bonds in the system, i.e., no π-π stacking. Low dynamic bonding rate $p_{create}/p_{break} = 2$ results in 6%–30% of maximum possible number of dynamic bonds depending on incompatibility and thus corresponds to weak π-π interaction. High dynamic bonding rate $p_{create}/p_{break} = 10$ leads to 60%–80% of the maximum possible number of dynamic bonds, which can interpreted as strong π-π interaction. The Flory-Huggins parameter χ_{AB} varied from 0 to 12. The main chain stiffness was fixed at $K_A = 12 k_b T/rad^2$ in this section.

Fig. 3(a) presents the phase diagram in χ_{AB} versus p_{create}/p_{break} coordinates, along with the simulation snapshots for each obtained type of morphology: disordered (black squares), cylinders (red circles), lamellae (full blue triangles) and distorted lamellae (empty blue triangles). The same morphologies are shown in more details in ESI, Figs. S1, S2, S4 and S5. First of all, systems with low χ_{AB} and weak π-π stacking exhibit no particular order. Similar to Fig. 2, increasing incompatibility between thiophene and side chains up to $\chi_{AB} \approx 4.5$ leads to the formation of hexagonal packed cylinder phase. Intermediate π-π stacking also stabilizes this phase at $\chi_{AB} = 0$ (Fig. 3(c)). In this phase, the core of the cylindrical aggregate is formed by the thiophene chains interconnected by rare dynamic bonds (see details in ESI, Fig. S3). All side chains are pushed out into the space between the aggregates. The same morphology was previously obtained by Marsh[30] in mesoscopic model of thiophene-based oligomers with side chains arranged on one side of the backbone. Thus, the presence of the HEX phase is the consequence of the absence of a torsion potential in our model. On one hand, the fibrillar phase in P3HT has different structure[65,66]. On the other hand, the obtained results may illustrate self-assembly in terthiophene–thieno[3,4-c]pyrrole-4,6-dione based conjugated polymers (P3TTPD) with different side chain orientation. P3TTPD is a comb-like polymer with two side chains on the thieno[3,4-c]pyrrole-4,6-dione (TPD) unit. Since P3TTPD and P3HT are similar in chemical composition (but with different chain structure), these polymers correspond to the same value of the parameter χ_{AB} and, as a result, the same horizontal line in the phase diagram (Fig. 3). Moreover, due to the different mutual orientation of the side chains in P3TTPD, "from each

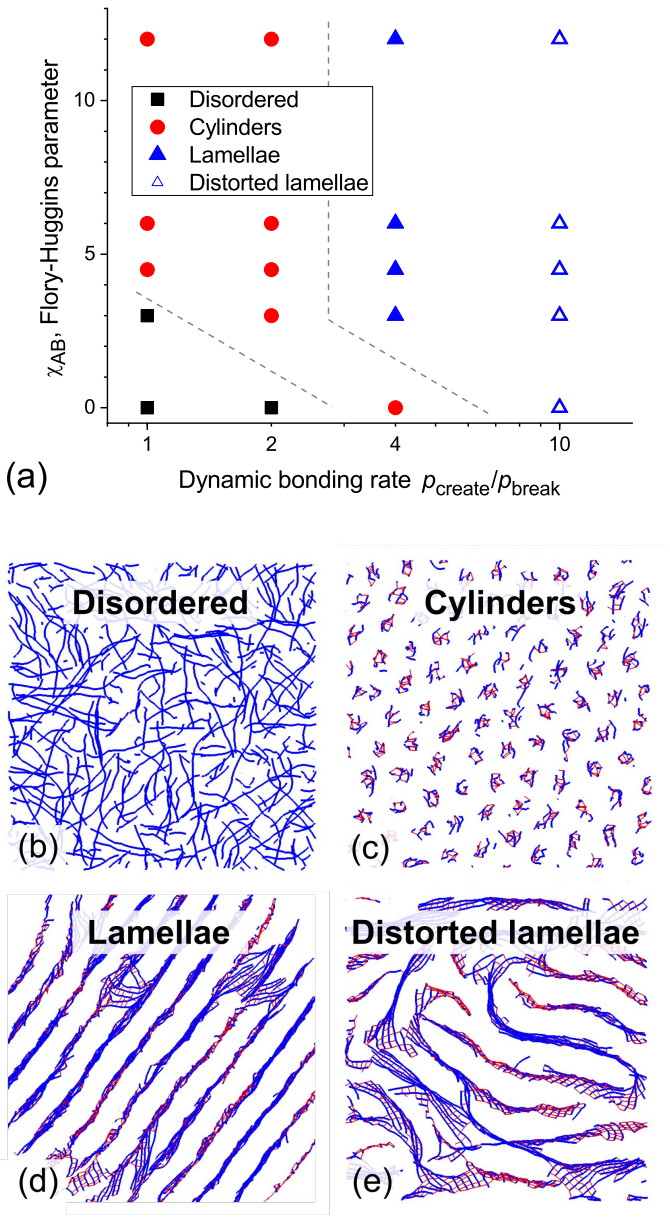

Fig. 3 (a) Phase diagram of equilibrated systems at various dynamic bonding rate p_{create}/p_{break} and Flory-Huggins parameter χ_{AB} of the main and side chains. Dash lines show the approximate positions of boundaries between phases. Snapshots of obtained morphologies: (b) disordered, (c) cylinders, (d) lamellae, and (e) distorted lamellae. The snapshots show only thiophene chains (blue) and dynamic non-covalent bonds between them (red), while side chains were not shown. The angle stiffness of the main chains $K_A = 12 k_b T/rad^2$. The value of $\chi_{AB} = 3$ corresponds to the case of P3HT (see ESI).

Molecular Systems Design & Engineering Accepted Manuscript

View Article Online
DOI: 10.1039/D0ME00034E

Published on 09 June 2020. Downloaded by Uppsala University on 6/13/2020 1:36:52 PM.

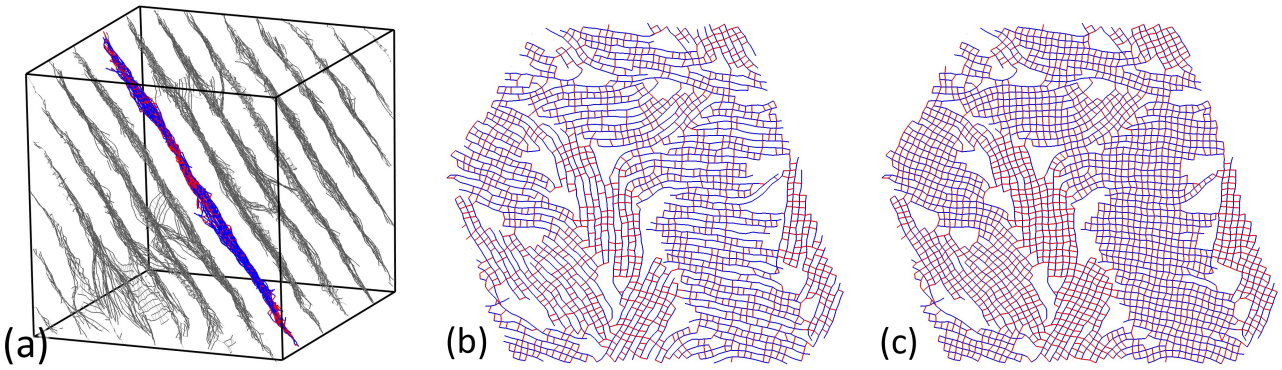

Fig. 4 Organisation of thiophene chains in a lamella. (a) The simulation box with the selected lamella. (b) Snapshot of the selected lamella (blue - thiophene chains, red - dynamic non-covalent bonds). (c) The same lamella after the empirical reconstruction of possible π-π bonds.

other" and "towards each other" (outward and inward), different P3TTPD series have different degrees of co-planarity. The outward series of P3TTPD has a higher co-planarity of the thiophene rings than the inward series. A high degree of co-planarity of the thiophene rings leads to the formation of more π-π bonds between polymer chains and vice versa, which corresponds to different regions of the phase diagram. Indeed, due to this structural feature, lamellar morphology is formed in the samples of the outward series of P3TTPD (as in the case of P3HT), and cylindrical morphology is formed in the inward series[56], which our model illustrates well.

At higher dynamic bonding rates, the system switches to lamellar morphology (see Fig. 3(d)). In this state the thiophene chains form large stacks within each lamella (see Fig. 4). Side chains fill the gaps between these planes (detailed structures are shown in ESI, Fig. S4). On average, these stacks contain 10–20 thiophene chains, and exhibit moderate longitudinal alignment together with high transverse directional order. Different stacks inside one lamella are not well aligned to each other, as well as stacks from different lamellas. Presumably, larger stacks may be formed in our model as well as stacks in one lamella may align in a single direction. However, simulation time required for re-alignment of stacks may be enormous, and an arbitrary box size may be incompatible with such alignment. Also, stacks from neighbour lamellae do not form larger aggregates in our model due to the softness of the side chains together with its random orientation towards the lamellae. The inclusion of torsion potentials presumably will lead to the interdigitation of side chains, which in turn may lead to the mutual alignment of stacks in neighbor lamellae.

Unexpectedly, the further increase of dynamic bonding rate does not improve the lamellar structure. Instead, it leads to the formation of distorted lamellar morphology, in which the general lamellar structure remains, but the stacks tend to bend, and a significant amount of stacks participate in more than one lamella at a time (Fig. 3(e)). As a result, there is no particular lamellar plane direction, and the system loses long-range order. At the same time, the average interlayer distance remains the same as in regular lamellar phase (detailed structures are shown in ESI, Fig. S5).

We computed static structure factors $S(q)$ for the observed morphologies in order to characterize its characteristic spatial scales more precisely. Fig. 5 shows $S(q)$ separately for thiophene and side chains in the range of $q/2\pi$ between $1/30\sigma^{-1}$ and $1\sigma^{-1}$, according to the box size. In the disordered system (Fig. 5(a)), the single smooth peak at $q/2\pi \sim 0.35\sigma^{-1}$ (wavelength $\lambda \sim 2.86\sigma \sim 16.3$Å) corresponds to the mean distance between thiophene chains. The same peaks were found in other phases, which corresponds to the mean distance between fibrils in the cylinder phase (Fig. 5(b)) and to the mean interlamellar distance in lamellar phases (Fig. 5(c) and (d)). In the latter case, it is the same peak as the (100) peak in SAXS measurements[7]. Fig. 5(b–d) shows secondary peaks with positions relating to the primary peak q^* as $q^* : 3^{1/2}q^* : 4^{1/2}q^* : 7^{1/2}q^*$ (Fig. 5(b)), $q^* : 2q^* : 3q^*$ (Fig. 5(c)), which is typical for hexagonal packed cylinders and lamellae, correspondingly[7,67].

Additional analysis of chain ordering is shown in ESI, Section S4.

The investigation of the effect of main chain length on the phase diagram shown the same results for chain lengths 20 and 40 (see ESI, Section S5 for details).

3.3 Effect of dynamic bonding in chemically homogeneous systems

Finally, we investigated in details the ability of the model to represent self-assembly in the systems without chemical incompatibility between main and side chains ($\chi_{AB} = 0$). For this purpose, we equilibrated systems with various main chain rigidities K_A and dynamic bonding rates $p_{\text{create}}/p_{\text{break}}$. Phase diagram for this setup contains disordered, cylindric, and distorted lamellar phases, as shown in Fig. 6. As well as in the case before, the formation of dynamic non-covalent bonds results in the self-assembly of the main chains into cylinders and, at higher $p_{\text{create}}/p_{\text{break}}$, into lamellae. The larger the persistent length of the main chains, the lower amount of dynamic bonds required for the predominance of ordered phases. Comparing the effect of the formation of dynamic bonds with the effect of chemical incompatibility, we could note the following two differences. On the large scale, the formation of dynamic bonds gives both cylindrical and lamellar phases. The latter one was not obtained without dynamic bonds at any

Molecular Systems Design & Engineering Accepted Manuscript

View Article Online
DOI: 10.1039/D0ME00034E

Published on 09 June 2020. Downloaded by Uppsala University on 6/13/2020 1:36:52 PM.

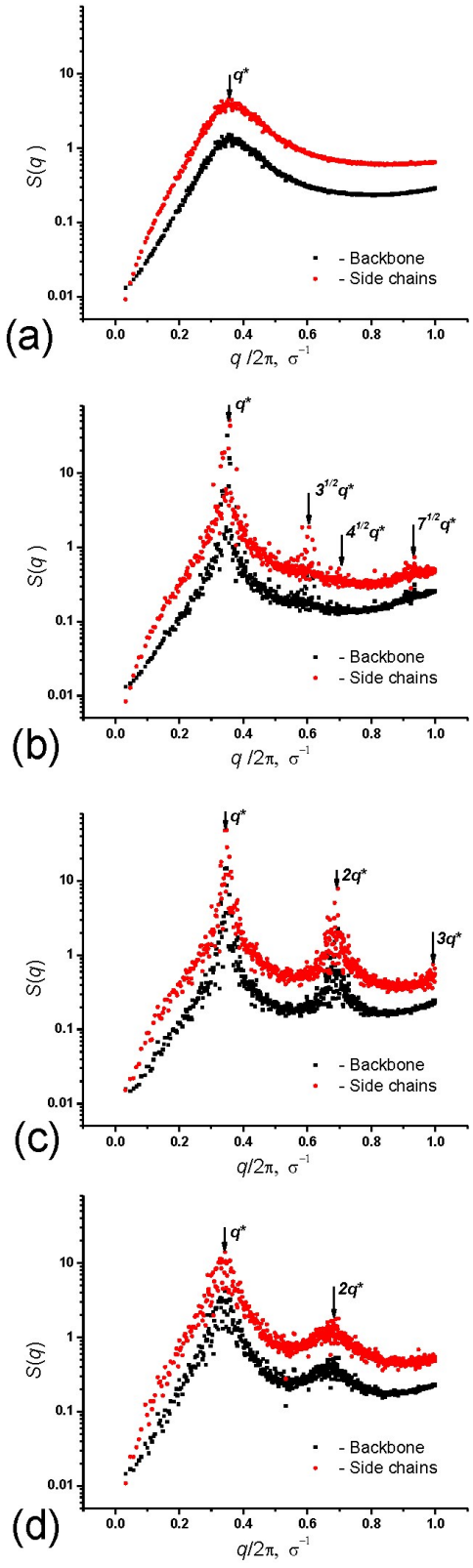

Fig. 5 The structural factors $S(q)$ of the observed morphologies: (a) disordered phase, (b) HEX phase, (c) lamellar phase with strong order, (d) lamellar phase with weak order.

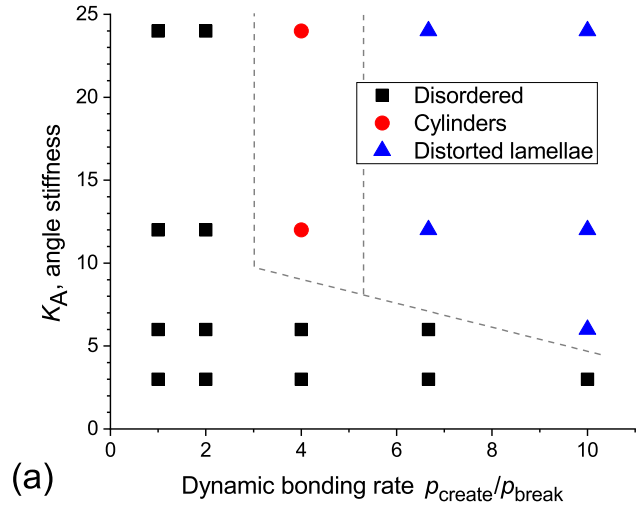

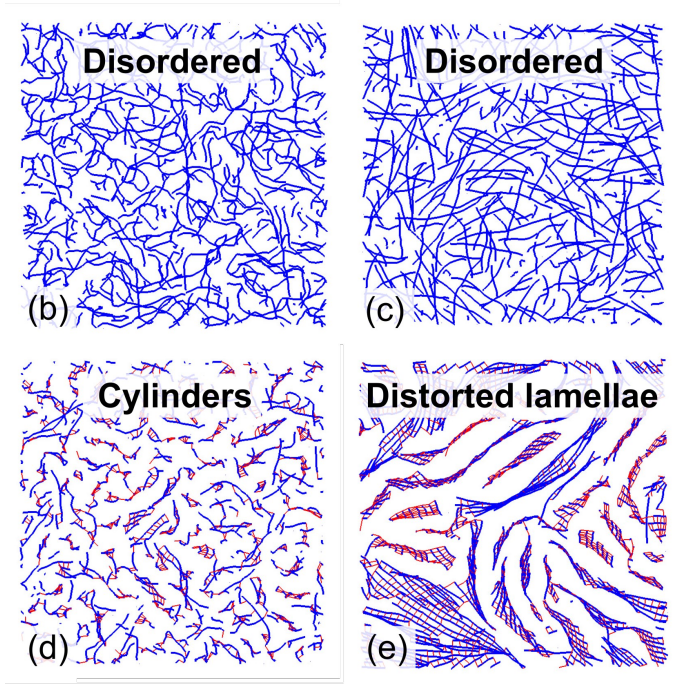

Fig. 6 (a) Phase diagram of equilibrated systems at various dynamic bonding rate $p_{\text{create}}/p_{\text{break}}$ and angle stiffness K_A of the main chains. Dash lines show the approximate positions of boundaries between phases. Snapshots of obtained morphologies: (b) disordered, $K_A = 3k_bT/rad^2$, (c) disordered, $K_A = 24k_bT/rad^2$, (d) cylinders, and (e) distorted lamellae. The snapshots show only main chains (blue) and dynamic non-covalent bonds between them (red), while side chains were not shown.

Molecular Systems Design & Engineering Accepted Manuscript

View Article Online
DOI: 10.1039/D0ME00034E

Published on 09 June 2020. Downloaded by Uppsala University on 6/13/2020 1:36:52 PM.

reasonable χ_{AB}. On the small scale, the formation of dynamic bonds results in additional ordering of the chains in single lamella into stacks, which is impossible to observe in systems with solely chemical incompatibility.

4 Conclusions and outlook

In this paper, we propose a mesoscale model of conjugated polymer matrix with dynamic bonding, reproducing π-π stacking. This model allows thiophene rings to form stacks, whose existence was previously shown experimentally. In turn, thiophene stacking leads to the ordering of the system into cylindrical, lamellar or distorted lamellar phases, depending on the main chain persistence length, chemical incompatibility of the polymer components, and non-covalent bond strength. Disordered phase occurs at low persistence length and low incompatibility. At higher persistence lengths, intrinsic to P3HT polymer, both dynamic bonding and incompatibility of polymer components allow the formation of hexagonal cylinder and lamellar phases. Unlike previous models without π-π stacking, our model leads to self-assembly of the polymer chains into large stacks with strong alignment due to dynamic bonding. In turn, these stacks form lamellae, which is in good agreement with the known experimental data.

Summarizing, we believe that the inclusion of π-π stacking into DPD method via dynamic bonding mechanism in our model is the next step towards realistic large scale simulations of polythiophene composites. As shown above, dynamic bonding allows to simulate the π-π stacking driven self-assembly of polythiophene-like polymers, which seems to be the initial phase of the crystallization process of such compounds. The model can be tuned to reproduce the morphology features of individual material via dynamic bonding parameters. Currently, our model does not include the potentials required for chain regioregularity, which is obtained in other models[30,34]. Regioregularity is one of the possible mechanisms of mutual alignment of chains pertaining to neighboring lamellae. Thereby the corresponding future expansion of the model will supposedly allow to simulate self-assembly of polycrystalline structure in P3HT melts more realistically. This is important for constructing large full-atomic material models (using the reverse mapping procedure[52,64]) based on equilibrated mesoscopic models of conjugated polymers matrices. At the same time, our model is not limited to P3HT compounds. In principle, any compound of the common nature can be translated into mesoscopic representation compatible with our approach. It opens up the possibilities to investigate the influence of non-covalent bonding in the self-assembly of a wide range of π-conjugated polymers.

Conflicts of interest

There are no conflicts to declare.

Acknowledgements

The financial support of the Russian Foundation for Basic Research (project 19-53-52004), the Ministry of Science and Technology of Taiwan (Project MOST 108-2923-E-002-001-MY3) and Ministry of Science and Higher Education of the Russian Federation are highly appreciated. The research is carried out using the equipment of the shared research facilities of HPC computing resources at Lomonosov Moscow State University.

The authors would like to thank V.A. Ivanov for constructive criticism of the manuscript.

Notes and references

1 K. M. Coakley and M. D. McGehee, Chemistry of Materials, 2004, **16**, 4533–4542.
2 L. Lu, T. Zheng, Q. Wu, A. M. Schneider, D. Zhao and L. Yu, Chem. Rev., 2015, **115**, 12666–12731.
3 S. H. Mir, L. A. Nagahara, T. Thundat, P. Mokarian-Tabari, H. Furukawa and A. Khosla, J. Electrochem. Soc., 2018, **165**, B3137–B3156.
4 J. R. Sheats, J. Mater. Res., 2004, **19**, 1974–1989.
5 A. J. Heeger, Advanced Materials, 2014, **26**, 10–28.
6 S. R. Puniredd, W. Pisula and K. Müllen, in Handbook of Organic Materials for Optical and (Opto)electronic Devices, Elsevier, 2013, pp. 83–101.
7 Z. Wu, A. Petzold, T. Henze, T. Thurn-Albrecht, R. H. Lohwasser, M. Sommer and M. Thelakkat, Macromolecules, 2010, **43**, 4646–4653.
8 C. M. Wolf, K. H. Kanekal, Y. Y. Yimer, M. Tyagi, S. Omar-Diallo, V. Pakhnyuk, C. K. Luscombe, J. Pfaendtner and L. D. Pozzo, Soft Matter, 2019, **15**, 5067–5083.
9 H. W. Ro, B. Akgun, B. T. O'Connor, M. Hammond, R. Joseph Kline, C. R. Snyder, S. K. Satija, A. L. Ayzner, M. F. Toney, C. L. Soles and D. M. DeLongchamp, Macromolecules, 2012, **45**, 6587–6599.
10 P. Kohn, Z. Rong, K. H. Scherer, A. Sepe, M. Sommer, P. Müller-Buschbaum, R. H. Friend, U. Steiner and S. Hüttner, Macromolecules, 2013, **46**, 4002–4013.
11 L. Mandelkern, Crystallization of Polymers, Cambridge University Press, Cambridge, UK, 2nd edn., 2011.
12 M. Zhang, B.-H. Guo and J. Xu, Crystals, 2017, **7**, 4–37.
13 Progress in Understanding of Polymer Crystallization, ed. G. Reiter and G. R. Strobl, Springer, 2007.
14 H. Meyer and F. Müller-Plathe, Macromolecules, 2002, **35**, 1241–1252.
15 Y. Termonia, Biomacromolecules, 2004, **5**, 2404–2407.
16 T. Yamamoto, Polymer, 2009, **50**, 1975–1985.
17 J.-U. Sommer and C. Luo, J. Polym. Sci. B Polym. Phys., 2010, **48**, 2222–2232.
18 X.-B. Zhang, Z.-S. Li, Z.-Y. Lu and C.-C. Sun, Macromolecules, 2002, **35**, 106–111.
19 T. Verho, A. Paajanen, J. Vaari and A. Laukkanen, Macromolecules, 2018, **51**, 4865–4873.
20 K. Hagita, S. Fujiwara and N. Iwaoka, J. Chem. Phys., 2019, **150**, 074901.
21 G. W. Heffner and D. S. Pearson, Macromolecules, 1991, **24**, 6295–6299.
22 B. Cesar, M. Rawiso, A. Mathis and B. François, Synth. Met., 1997, **84**, 241–242.
23 J. Sponer, P. Jurecka, I. Marchan, F. J. Luque, M. Orozco and P. Hobza, Chemistry, 2006, **12**, 2854–2865.

Molecular Systems Design & Engineering Accepted Manuscript

View Article Online
DOI: 10.1039/D0ME00034E

Published on 09 June 2020. Downloaded by Uppsala University on 6/13/2020 1:36:52 PM.

24 R. Zhao and R.-Q. Zhang, Phys. Chem. Chem. Phys., 2016, **18**, 25452–25457.

25 R. S. Paton and J. M. Goodman, J. Chem. Inf. Model., 2009, **49**, 944–955.

26 R. Zhou, Modeling of Nanotoxicity: Molecular Interactions of Nanomaterials with Bionanomachines, Springer, 2015.

27 C.-K. Lee, C.-W. Pao and C.-W. Chu, Energy Environ. Sci., 2011, **4**, 4124–4132.

28 D. Dudenko, A. Kiersnowski, J. Shu, W. Pisula, D. Sebastiani, H. W. Spiess and M. R. Hansen, Angew. Chem. Int. Ed. Engl., 2012, **51**, 11068–11072.

29 S. Obata and Y. Shimoi, Phys. Chem. Chem. Phys., 2013, **15**, 9265–9270.

30 H. S. Marsh, E. Jankowski and A. Jayaraman, Macromolecules, 2014, **47**, 2736–2747.

31 C. Du, Y. Ji, J. Xue, T. Hou, J. Tang, S.-T. Lee and Y. Li, Sci. Rep., 2015, **5**, 16854.

32 S. E. Root, S. Savagatrup, C. J. Pais, G. Arya and D. J. Lipomi, Macromolecules, 2016, **49**, 2886–2894.

33 K. N. Schwarz, T. W. Kee and D. M. Huang, Nanoscale, 2013, **5**, 2017–2027.

34 E. D. Miller, M. L. Jones, M. M. Henry, P. Chery, K. Miller and E. Jankowski, Polymers, **10**, 1305.

35 C. Greco, A. Melnyk, K. Kremer, D. Andrienko and K. C. Daoulas, Macromolecules, 2019, **52**, 968–981.

36 M. M. Henry, M. L. Jones, S. D. Oosterhout, W. A. Braunecker, T. W. Kemper, R. E. Larsen, N. Kopidakis, M. F. Toney, D. C. Olson and E. Jankowski, J. Phys. Chem. C, 2017, **121**, 26528–26538.

37 P. Komarov, P. Baburkin, V. Ivanov, S.-A. Chen and A. Khokhlov, Molecular Systems Design & Engineering, 2019, **4**, 390–395.

38 R. D. Groot and P. B. Warren, The Journal of Chemical Physics, 1997, **107**, 4423–4435.

39 A. A. Markina, V. A. Ivanov, P. V. Komarov, A. R. Khokhlov and S.-H. Tung, J. Phys. Chem. B, 2017, **121**, 7878–7888.

40 D. S. Dolgov, T. E. Grigor'ev, A. I. Kulebyakina, E. V. Razuvaeva, R. A. Gumerov, S. N. Chvalun and I. I. Potemkin, Polym. Sci. Series A, 2018, **60**, 902–910.

41 J. Sjöqvist, M. Linares, K. V. Mikkelsen and P. Norman, The Journal of Physical Chemistry A, 2014, **118**, 3419–3428.

42 C. Cozza, M. Bonomi and A. Pietropaolo, Journal of Chemical Theory and Computation, 2018, **14**, 5441–5445.

43 O. A. Guskova, in Quantum Systems in Physics, Chemistry, and Biology, Springer International Publishing, 2017, pp. 209–230.

44 P. J. Hoogerbrugge and J. M. V. A. Koelman, Europhysics Letters (EPL), 1992, **19**, 155–160.

45 J. M. V. A. Koelman and P. J. Hoogerbrugge, Europhysics Letters (EPL), 1993, **21**, 363–368.

46 P. Español and P. Warren, Europhysics Letters (EPL), 1995, **30**, 191–196.

47 P. Komarov, A. Markina and V. Ivanov, Chem. Phys. Lett., 2016, **653**, 24–29.

48 A. Markina, V. Ivanov, P. Komarov, S. Larin, J. M. Kenny and S. Lyulin, J. Polym. Sci. B Polym. Phys., 2017, **55**, 1254–1265.

49 A. V. Berezkin and Y. V. Kudryavtsev, Macromolecules, 2011, **44**, 112–121.

50 C. Svaneborg, Comput. Phys. Commun., 2012, **183**, 1793–1802.

51 P. V. Komarov, O. E. Zaborina, T. P. Klimova, V. I. Lozinsky, P. G. Khalatur and A. R. Khokhlov, Chem. Phys. Lett., 2016, **661**, 219–223.

52 D. V. Guseva, V. Y. Rudyak, P. V. Komarov, A. V. Sulimov, B. A. Bulgakov and A. V. Chertovich, J. Polym. Sci. B Polym. Phys., 2018, **56**, 362–374.

53 S. Thomas, M. Alberts, M. M. Henry, C. E. Estridge and E. Jankowski, J. Theor. Comput. Chem., 2018, **17**, 1840005.

54 C. Li and A. Strachan, Journal of Polymer Science Part B: Polymer Physics, 2015, **53**, 103–122.

55 J. Gross, M. Ivanov and W. Janke, J. Phys. Conf. Ser., 2016, **750**, 012009.

56 C.-A. Chen, P.-C. Yang, S.-C. Wang, S.-H. Tung and W.-F. Su, Macromolecules, 2018, **51**, 7828–7835.

57 A. V. Chertovich, V. A. Ivanov, A. R. Khokhlov and J. Bohr, J. Phys.: Condens. Matter, 2003, **15**, 3013–3027.

58 A. V. Berezkin, P. G. Khalatur and A. R. Khokhlov, J. Chem. Phys., 2003, **118**, 8049–8060.

59 D. V. Guseva, Y. V. Kudryavtsev and A. V. Berezkin, J. Chem. Phys., 2011, **135**, 204904.

60 A. V. Berezkin and Y. V. Kudryavtsev, J. Chem. Phys., 2014, **141**, 194906.

61 V. Y. Rudyak, A. A. Gavrilov, D. V. Guseva and A. V. Chertovich, Macromolecular Theory and Simulations, 2017, **26**, 1700015.

62 A. A. Gavrilov and A. V. Chertovich, Macromolecules, 2017, **50**, 4677–4685.

63 V. Y. Rudyak, A. A. Gavrilov, E. Y. Kozhunova and A. V. Chertovich, Soft Matter, 2018, **14**, 2777–2781.

64 D. V. Guseva, V. Y. Rudyak, P. V. Komarov, B. A. Bulgakov, A. V. Babkin and A. V. Chertovich, Polymers, 2018, **10**, 792.

65 Y. Han, Y. Guo, Y. Chang, Yingfeiand Geng and Z. Su, Macromolecules, 2014, **47**, 3708–3712.

66 S. Lee, H. Jeon, M. Jang, K.-Y. Baek and H. Yang, ACS Appl. Mater. Interfaces, 2015, **7**, 1290–1297.

67 I. Hamley and V. Castelletto, in Soft Matter Characterization, ed. R. Borsali and R. Pecora, Springer Netherlands, Dordrecht, 2008, vol. 13, pp. 1021–1081.

Molecular Systems Design & Engineering Accepted Manuscript

View Article Online
DOI: 10.1039/D0ME00034E

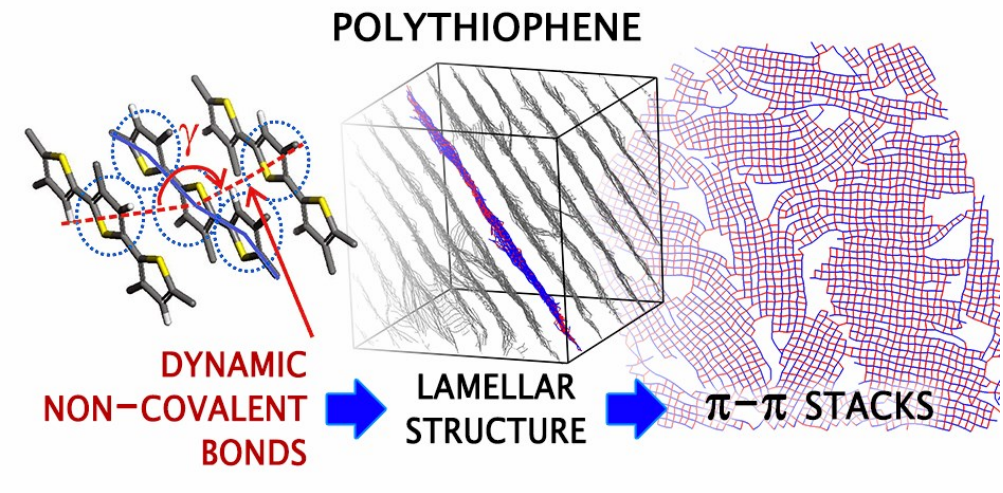

80x39mm (300 x 300 DPI)

Published on 09 June 2020. Downloaded by Uppsala University on 6/13/2020 1:36:52 PM.

Molecular Systems Design & Engineering Accepted Manuscript

View Article Online
DOI: 10.1039/D0ME00034E

TOC Entry

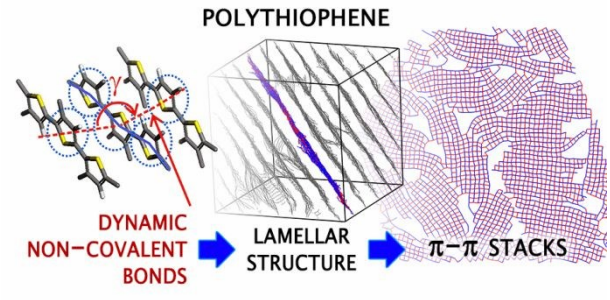

Accounting for π-π interactions between conjugated polymers molecules via dynamic bonds allows its self-assembly into lamellar morphology with π-π stacks

Published on 09 June 2020. Downloaded by Uppsala University on 6/13/2020 1:36:52 PM.

Molecular Systems Design & Engineering Accepted Manuscript